Eccentric binary neutron star mergers

Roman Gold,[1,2,3] Sebastiano Bernuzzi,[1] Marcus Thierfelder,[1] Bernd Brügmann,[1] and Frans Pretorius[2]

[1] *Theoretisch-Physikalisches Institut, Friedrich Schiller Universität Jena, Max-Wien-Platz 1, 07743 Jena, Germany*
[2] *Department of Physics, Princeton University, Princeton, NJ 08544, USA*
[3] *Department of Physics, University of Illinois at Urbana-Champaign, Urbana, Illinois 61801*

(Dated: September 12, 2012)

Neutron star binaries offer a rich phenomenology in terms of gravitational waves and merger remnants. However, most general relativistic studies have been performed for nearly circular binaries, with the exception of head-on collisions. We present the first numerical relativity investigation of mergers of eccentric equal-mass neutron-star binaries that probes the regime between head-on and circular. In addition to gravitational waves generated by the orbital motion, we find that the signal also contains a strong component due to stellar oscillations (f-modes) induced by tidal forces, extending a classical result for Newtonian binaries. The merger can lead to rather massive disks on the order of 10% of the total initial mass.

I. INTRODUCTION.

Binary neutron star (NSNS) mergers are among the most promising sources of gravitational waves (GWs) for ground-based interferometers, as well as plausible candidates for the central engine of short-gamma-ray-burst (sGRB). One of the main tools for studying NSNS mergers is numerical relativity, which experienced a dramatic development in the last ten years achieving important results in NSNS and recently also for black hole-neutron star (BHNS) simulations, e.g. [1–3].

In numerical relativity NSNS mergers have been almost exclusively studied for circularized initial data. The exceptions are head-on collisions [4, 5], and the low eccentricity ($e \approx 0.2$) orbits of [6] also recall the residual eccentricity of quasi-circular data [7]. (See [8] for a nearly head-on Newtonian simulation with radiation reaction.) So far, there are no numerical studies exploring the range from small to large eccentricity. One reason for this is an expectation that the dominant population of NSNS mergers in the universe results from evolution of primordial stellar binaries. For such systems, residual eccentricity at the time of merger is expected to be low. For example, a recent investigation suggests that only between 0.2% and 2% of this class of mergers detectable by Advanced LIGO/VIRGO will have eccentricity $e > 0.01$ (and $e \lesssim 0.05$) [9].

However, recent studies have suggested there may be a significant population of compact object binaries formed via dynamical capture in dense stellar environments [10, 11], and a large fraction of these would merge with high eccentricity. In [11] the number of dynamical capture NSNS mergers in globular clusters (GCs) was calculated, finding a redshift dependent rate that peaks at $50/\mathrm{yr}/\mathrm{Gpc}^3$ at $z = 0.7$, decreasing to $30/\mathrm{yr}/\mathrm{Gpc}^3$ today. This is large enough to account for a significant fraction of sGRBs, assuming NSNS mergers are their progenitors. However, the calculated merger rate is quite sensitive to the fraction f of NSs in the core, scaling as $\sim f^2$, and their model (using M15 as the prototype GC) did not account for NS loss due to natal kicks. A recent simulation of M15 by [12] fit to observations and assuming a modest NS retention fraction of 5%, found roughly 1/4 fewer NSs within the central 0.2 pc compared to an earlier study that did not account for kicks [13], implying the rates of [11] could be overestimates by an order of magnitude due to this effect. On the other hand, the 5% retention fraction used in [12] may be too low, as observations of GCs suggest it could be as large as 20% [14]. Furthermore, the model of [11] did not take into account other channels that could lead to high eccentricity binary merger within a Hubble time, such as Kozai resonance in a triple system [15]. Observations of sGRBs have also suggested there are different progenitors for sGRBs that exhibit so called extended emission and those that do not [16]; an obvious speculation of the cause of the bimodality is primordial vs. dynamical capture NSNS mergers.

Although the issue of event rates is unsettled, we expect smaller but not negligible rates for eccentric binaries in the overall population. We therefore posit their existence, and ask what theory predicts for the evolution and the gravitational waves of eccentric NSNS binaries.

Eccentric mergers can lead to a rich phenomenology in GWs and the merger remnant. The properties of the accretion disk formed as a product of the merger are so far poorly understood, even though there is the possibility of massive disk production, $M_\mathrm{d} \sim 10\%$ of the total initial binary mass. Recent results [17] for BHNS systems indicate a strong variability in properties of the merger remnant as a function of the eccentricity. The gravitational waveforms significantly differ from the chirp signal of quasi-circular inspirals that feature slowly increasing amplitude. During eccentric orbits, each periastron passage leads to a burst of radiation, first studied using Newtonian orbits together with leading order relativistic expressions for radiation and the evolution of orbital parameters [18, 19], and more recently with numerical simulations of BHBH and BHNS systems in full general relativity [17, 20–23]. An important Newtonian result concerning NSNS (or BHNS) is that eccentricity leads to tidal interactions that can excite oscillations of the stars, which in turn generate their own characteristic GW sig-

nal [24] (see also [11, 25]). In some cases the GWs can be dominated by these non-orbital contributions [24]. Neither the orbital nor stellar GWs have been studied so far for eccentric NSNS orbits in general relativity.

In this work we present the first numerical relativity investigation of (highly) eccentric NSNS mergers (see Refs. [11, 26] for studies of similar systems in Newtonian gravity). We consider an equal-mass binary at fixed initial separation and vary the initial eccentricity. Three models are discussed that are representative of the different orbital phenomenology observed: direct plunge, merger after a close encounter, and multiple encounters. We analyze the emitted GW and the dynamics in the matter, and characterize the basic properties of the merger remnant.

II. NUMERICAL METHOD.

We performed numerical simulations in 3+1 numerical relativity solving the Einstein equations coupled to a perfect fluid matter model (no magnetic fields). We employed the BAM code [27, 28], which we recently extended to general relativistic hydrodynamics [29]. Referring to [28, 29] for details and further references, we solve the BSSN formulation in the moving puncture gauge coupled to matter in flux-conservative form. Metric and matter fields are discretized in space on 3D Cartesian meshes refined with the technique of moving boxes. Time integration is performed with the method-of-lines using a 3rd order Runge-Kutta scheme. Derivatives of metric fields are approximated by fourth-order finite differences, while a high-resolution-shock-capturing scheme based on the local-Lax-Friedrich central scheme and the convex-essentially-non-oscillatory reconstruction is adopted for the matter. Neutron star matter is modeled with a polytropic equation of state with adiabatic index $\Gamma = 2$. GWs are extracted at finite coordinate radius, $r \sim 90M$ ($180M$ for Model 3), by using the Newman-Penrose curvature scalar, Ψ^4, where $M = 2.8M_\odot$ is the gravitational mass of the system.

Although the problem of posing initial data to the Einstein equations by solving the constraints is in principle well understood, there is no ready-made prescription for eccentric NSNS that is of interest here (although see the recent work in Refs. [30, 31]). We postpone the solution of the constraint equations and instead work with the following approximation. Initial data are set by superposing two boosted non-rotating stars with the same gravitational mass $1.4M_\odot$ at apoastron. Specifically, we (i) compute a relativistic spherical star configuration (TOV) of mass $M_\star = 1.4M_\odot$; (ii) obtain two boosted star configurations by performing the Lorentz transformation along the y-axis with parameters $\xi = (0, \pm\xi_y, 0)$; (iii) place the star centers at coordinate locations $(x_\pm, y, z) = (\pm 25\ M, 0, 0)$, respectively; (iv) add the 4-metric fields of the two spacetimes and subtract the flat metric in order to enforce asymptotical flatness; and (v) derive 3+1 decomposed initial data. The initial spatial metric is not conformally flat. The matter initial data are approximately irrotational and represent orbiting neutron stars near apoastron. The maximum constraint violation (at the center of the star) decays as $1/d$ as expected for the relatively large initial proper separation $d \sim 54.7M$ (compared to typical separations of quasi-circular initial data, e.g. Refs. [29, 32]). The constraint violation is at the level of the truncation error of the evolution scheme (see also the discussion in Refs. [6, 17]).

We performed a series of simulations for different initial boosts (i.e. Newtonian apoastron velocities), $\xi_y \in [0.01, 0.05]$. The eccentricity arising from these choices cannot be unambiguously quantified in GR. The Newtonian equivalent of these configurations would lead to eccentric elliptic orbits with eccentricities as listed in Tab. I. Newtonian circular orbits are obtained for $\xi_y \simeq 0.07$. The evolution of the orbital separation and the GW frequency suggest that the Newtonian values overestimate the eccentricities.

The grid consisted of five refinement levels with maximum spatial resolution $h \sim 0.15 - 0.2M_\odot$ and a Courant-Friedrichs-Lewy factor of 0.25. We have checked that varying the box size, $B \sim 200 - 400M$, has only minor effects on the orbits and the waves. For $\xi_y \lesssim 0.020$, within $1000M$ a merger and formation of a black hole occurred. Selected models were continued for $\sim 700M$ ($\sim 10ms$) after the merger in order to follow the accretion process on to the final black hole. During evolutions the largest violation of the rest-mass conservation occurs before collapse, $\Delta M_0/M_0 \sim 0.01$. Similarly the ADM mass was conserved up to 1%. The consistency of the results was assessed by convergence tests.

III. ORBITAL DYNAMICS.

We begin by reporting the orbital dynamics in selected models. See Fig. 1 for the star tracks as computed from the minimum of the lapse function [29].

In Model 1 ($\xi_y = 0.010$) the stars move almost directly towards each other, collide, then undergo prompt collapse to a black hole at $t = 423M$ with dimensionless spin parameter $a_{\rm BH} \sim 0.58$ and mass $M_{\rm BH} \sim 2.8M_\odot$. The resulting disk has negligible rest-mass, $M^d \lesssim 10^{-7}M_0$, which is at the level of the artificial atmosphere used for the numerical treatment of vacuum for the matter.

In Model 2 ($\xi_y = 0.020$) the stars come into contact but survive the first encounter. During contact matter is exchanged between the outer layers of the stars, see Fig. 2; The density weighted Newtonian vorticity is 10 times larger than for an irrotational NSNS binary. During a second encounter they merge forming a black hole at $t = 975M$ with initial $a_{\rm BH} \sim 0.79$ and mass $M_{\rm BH} \sim 2.2M_\odot$. In contrast to Model 1, there is a massive disk with $M^d = (0.15 \pm 0.02)M_\odot$ (the error estimate is based on five resolutions between $h \sim 0.15 - 0.2M_\odot$),

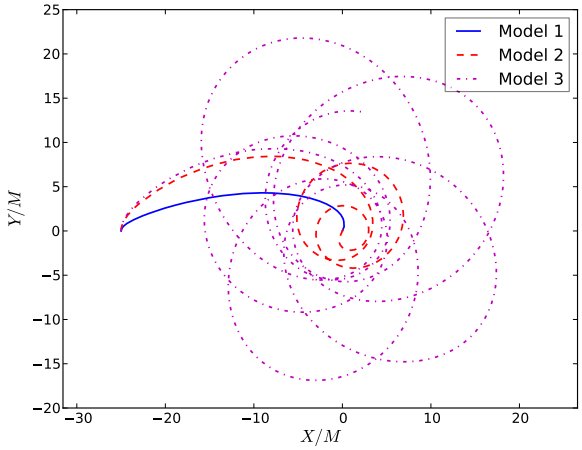

FIG. 1: Star tracks for Model 1, 2, and 3. The tracks of the second star can be inferred from symmetry.

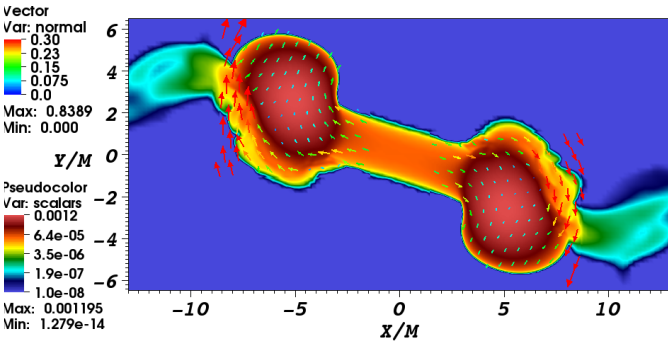

FIG. 2: Model 2 at $t = 553M$, shortly after the stars have touched and separated again. The rest-mass density (log-scale) and the three-velocity in the orbital plane are shown.

measured $100M$ after the formation of an apparent horizon. We find larger masses up to $M^d \sim 0.27M_\odot$ for intermediate models which are not discussed here in detail, see Tab. I. The accretion has increased the mass and spin to $M_{\rm BH} \sim 2.64M_\odot$ and $a_{\rm BH} \sim 0.81$. Prior to the onset of merger, for a time of $\approx 100M$ the binary approaches a nearly circular orbit where the separation remains close to a constant $\sim 5M$. This suggests a transition through a whirl regime as in BBH systems [17, 20–23, 33]. After the merger we observe quasi-periodic oscillations in the accretion flow at a frequency $\nu_{QPO} \sim 0.5kHz$ in the vicinity of the black hole.

In Model 3 ($\xi_y = 0.022$) multiple close passages with no matter exchange are observed. The two bodies do not merge during a simulation time of $t = 6400M$. The orbits show a significant periastron precession, leading to an overall rotation of the quasi-elliptical orbit of almost 90 degrees per encounter. Although the precession is highly relativistic, these encounters occur well outside the whirl regime.

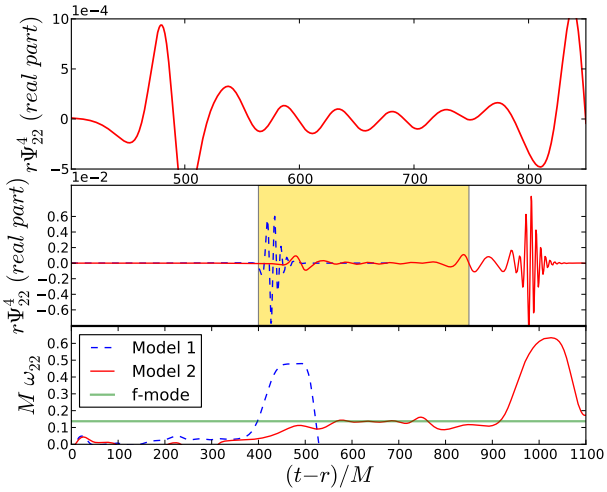

FIG. 3: Real part of the $r\,\Psi^4_{22}$ waveforms (central panel) and instantaneous gravitational wave frequency (bottom panel), $M\omega_{22}$, as a function of retarded time, $(t-r)/M$, for Models 1 and 2. The top panel shows a zoom in on the shaded region in the central panel for Model 2. The horizontal line in the bottom panel marks the perturbative f-mode frequency.

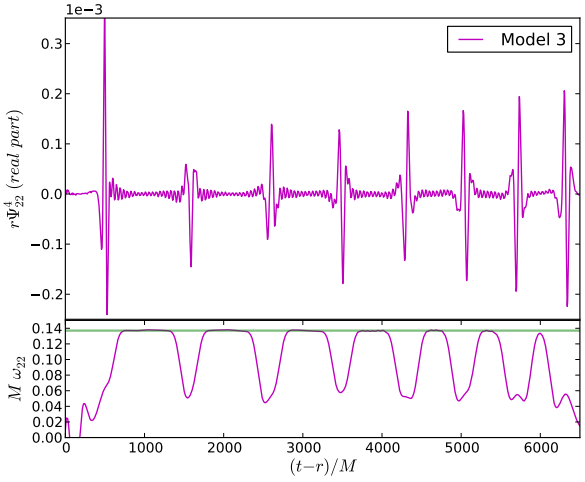

FIG. 4: Same as the central and bottom panels of Fig. 3 but for Model 3.

IV. WAVEFORMS.

The orbital motion of each model results in a characteristic gravitational wave signal. Figs. 3 and 4 display the $\ell = m = 2$ mode, Ψ^4_{22}, as well as the corresponding instantaneous gravitational wave frequency, $M\omega_{22}$, of the curvature scalar, which represents the main emission channel for the binary signal.

Waveforms from Model 1 are characterized by a peak at the merger and the subsequent quasi-normal-mode (QNM) ringing of the final black hole. The GW frequency of the QNM is $M\omega_{22} \sim 0.48$, compatible with the fundamental QNM frequency of the Kerr black hole com-

puted from the apparent horizon parameters, e.g. [34]. In fact, we find the value $\nu_{\rm QNM} \sim 5.9kHz$, which differs by 6% from the value obtained from the GW. Waveforms from Model 2 show a burst at retarded time $t-r \sim 500M$ related to the orbital dynamics [19], followed by a feature between $t-r \sim [800M-900M]$ akin to a transition through a whirl phase and the final merger signal around $t-r \sim 1000M$. In this case the QNM frequency is higher, $M\omega_{22} \sim 0.632$ ($\nu_{\rm QNM} \sim 7.6kHz$, 2% discrepancy). The waveforms from Model 3 exhibit several bursts corresponding to the periastron passages.

The key feature is that between the bursts one can observe high frequency signals in several GW-modes (e.g. for Model 2 at $t-r \sim [550M-750M]$). These are absent in the black hole case, but similar to Newtonian results [11], and qualitatively similar to BHNS mergers [17, 35]. This signature is progressively suppressed at lower eccentricities (larger ξ_y) and not observed for $\xi_y = 0.05$. Referring to Fig. 4, the $(2,2)$ GW frequency is dominated by several plateaus compatible with the f-mode frequency of the non-rotating star in isolation [36–38], $M\omega_{\rm f} \sim 0.137$ ($\nu_{\rm f} \sim 1.586kHz$), interrupted briefly by the close encounter bursts. In Model 2, the signal is mainly in the $(2,2)$ multipole; the $(2,0)$ multipole (not shown) also contains the signature (weaker in amplitude by a factor five). In contrast, in Model 3 the amplitude of the $(2,2)$ multipole is smaller in amplitude by a factor of three than the $(2,0)$ multipole, which is the main emission channel between the bursts (encounters).

The natural interpretation is that these GWs are produced by oscillations of the individual stars, which are tidally induced by the companion. Physically, the expectation is that the approximately head-on, zoom-part of the orbit is responsible for exciting axisymmetric $m=0$ modes, while in particular $m=2$ modes should arise from the approximately circular, partial whirl near periastron. The relative amplitude of the modes indicates the effectiveness of the different phases of the binary interaction to excite certain modes. Indeed the Newtonian analysis of Turner [24] indicates that a sufficiently close periastron passage (i.e. $e \lesssim 1$ for fixed apoastron) exerts a pulse-like tidal perturbation which excites the axisymmetric f-modes of the star, leading to a GW waveform dominated by the star oscillations rather then by the emission due to the orbital motion. Note that the phenomenon is different from a resonant tidal excitation, see e.g. [25, 39], which instead refer to the circular motion case.

If these waves indeed correspond to stellar f-modes, they should be detectable as oscillations of the stellar matter. Consider the projections of the rest-mass density of one of the stars onto the spherical harmonics, e.g. [37], $\rho_{\ell m} \equiv \int Y^*_{\ell m} \rho\, d^3x$, and perform an analysis of the spectrum. Results are reported in Fig. 5 for Model 2 and 3, where the $\rho_{22}(t)$ projections and their power spectral density (PSD) are shown. In both these (and in other intermediate) models we can clearly identify frequencies compatible with the linear f-mode, together with secondary peaks presumably due to nonlinear couplings and/or non-axisymmetric modes. Similar results are obtained for the projection ρ_{20}, while in this case the signal is strongly modulated by the orbital motion and contains a signature of the radial ($\ell = m = 0$) F-mode of the star from the beginning of the simulation.

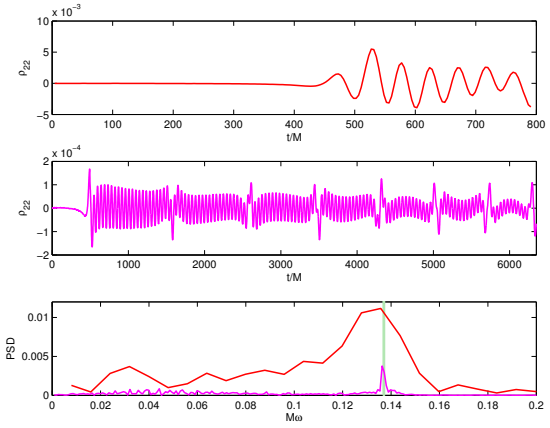

FIG. 5: Mode analysis. The panels display the $\ell = m = 2$ spherical-harmonic projection of the rest-mass density of one of the stars (Model 2 top, Model 3 center), and its power spectral density (PSD, bottom), where ν_f is marked. The green shaded area spans the perturbative values of the mode frequencies of star configurations A0-A1 in [36] (right-left).

In [36] the f-mode frequencies for different stellar models are given. In particular, the f-mode frequency is sensitive to the rotation of the star. Note that, given an uncertainty in the frequencies obtained from our simulations, we can derive an upper limit on the rotation of the star. In Model 2 the peak in the PSD corresponding to the f-mode frequency is too broad for a restrictive upper limit. The broadening is caused by the limited number of cycles due to the short signal. In Model 3 there are more cycles leading to a more accurate determination of the frequency. The latter lies between model A0 (non-rotating case) and A1 in [36]. We conclude that the individual neutron stars have lower values of rotational/potential energy T/W than model A1, which is given as $T/W = 0.02$. r-modes are thus not expected, but they may be present in the outer layers of Model 2; g-modes are absent here by construction.

The main observation is that f-modes are excited during the encounter, i.e. the f-mode is present in all models that survive the first encounter. The value for ν_f remains unchanged for different resolutions (see Fig. 6) and different initial data, demonstrating the robustness of our finding.

Finally, we discuss the properties of the merger remnant and the surrounding accretion disk for models with ξ_y between those of the previously discussed Models 1-3. In Tab. I initial parameters of the different models are listed together with merger time t_{AH}, horizon mass M_{BH}, and spin a_{BH}. The superscripts 0 and d denote times t_{AH} and $t^d \equiv t_{AH} + 100M$, respectively. The lat-

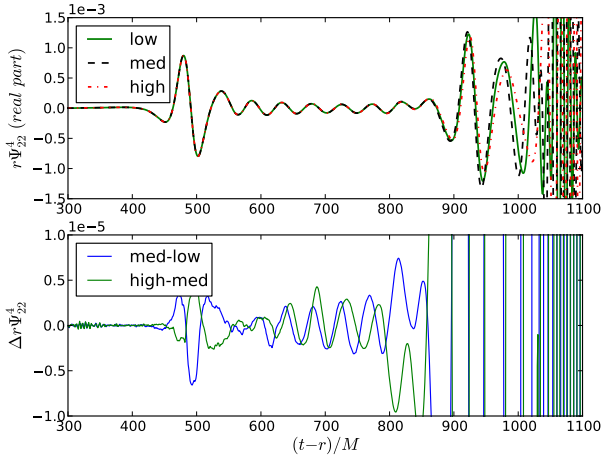

FIG. 6: Real part of the $r\Psi_{22}^4$ waveforms of Model 2 at three different resolutions. The differences are two orders of magnitude lower than the ν_f signal. At $t \gtrsim 900$ the phase error becomes large due to the highly sensitive whirl motion.

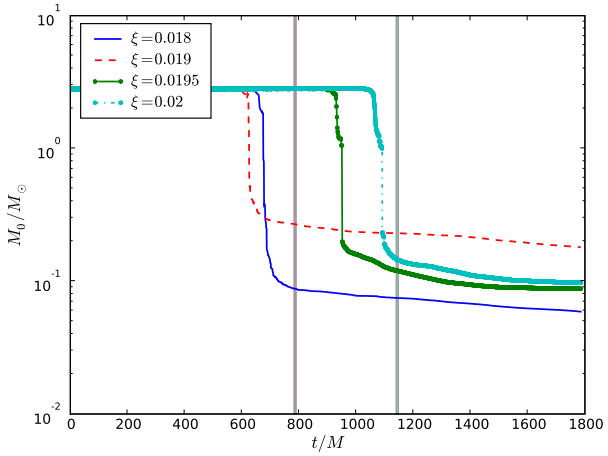

FIG. 7: Rest-mass density evolution of Model 2 and selected intermediate models. The vertical lines denote t_d for $\xi = 0.019$ and $\xi = 0.02$.

TABLE I: Summary of the merger remnant properties. Columns: initial data boost parameter, Newtonian eccentricity of the initial data, mass and spin of the final black hole at two different times as estimated from the apparent horizon, disk rest-mass, and accretion time. Errors are about 1 %.

ξ_y	e	$t_{\rm AH}/M$	$M^0_{\rm BH}$	$M^d_{\rm BH}$	$a^0_{\rm BH}$	$a^d_{\rm BH}$	$M^{\rm d}/M_\odot$	$\tau[\times 10^3]$
0.01	0.978	423	2.82	2.81	0.58	0.57	$<10^{-7}$	-
0.017	0.937	669	2.05	2.78	0.64	0.76	0.004	0.56M
0.0175	0.933	658	2.06	2.75	0.66	0.75	0.05	1.84M
0.0185	0.925	692	2.13	2.73	0.74	0.78	0.07	0.93M
0.019	0.921	616	2.14	2.54	0.71	0.75	0.27	2.72M
0.0195	0.917	643	2.02	2.60	0.72	0.79	0.20	0.47M
0.02	0.913	1077	2.05	2.61	0.70	0.81	0.18	1.81M

ter time is empirically motivated by an initial phase of rapid change in the merger properties. We find that after t^d the remnant and the disk are changing much more slowly. See Fig. 7 for the evolution of the rest-mass as a function of time for selected models. The results are in qualitative agreement with corresponding results in which constraint-satisfying initial data are used [40]. We find final spins of $0.75 < a^d_{BH} < 0.81$ for all models (except Model 1) and disk masses $M^d \gtrsim 0.18 M_\odot$ for $\xi_y \geq 0.019$. As found in [40], grazing encounters exhibit larger disk masses. In the early post-merger stages that we simulate, the accretion rate can be fit to an exponential function, which allows us to quote a characteristic accretion time scale τ. These values are given in the last column of Tab. I and range from $4ms$ to $30ms$.

V. CONCLUSION.

Mergers of eccentric NSNS binaries, although expected to be rare, could be very interesting sources for third generation GW detectors, in particular given the (in some respect) surprisingly strong and clear signal from orbit-induced stellar oscillations (OISOs). We find disk masses on the order $M^d \sim 0.2$ and remnant BH spins $a_{BH} \sim 0.8$. Due to the sensitive dependence of the binary evolution on orbital parameters, signals from OISOs could pose constraints on the equation of state. This motivates an extension of this work in the future to a more realistic equation of state including a quantification of the shock heating and the possibility of the formation of a hypermassive neutron star. Our study raises the question of to what extent a NS crust could tolerate such strong deformations. As also pointed out in [40] the crust may fail during the inspiral.

This study is preliminary in many aspects, but it represents a first step toward building GR models of eccentric binary neutron stars. We consider improved initial data and a more realistic matter model (see [31, 40]) to be the most important extensions. The present results are likely to be highly dependent on the compactness of the stars and on the mass ratio, thus these cases should be studied as well. Furthermore, even larger disk masses are expected for the unequal mass case which could be interesting for sGRB astrophysics. More work is required in these directions together with a detailed understanding of the eccentric NSNS population in the universe.

VI. ACKNOWLEDGMENTS.

We gratefully acknowledge helpful discussions with William East, Branson Stephens, and Kostas Kokko-

tas. This work was supported in part by DFG SFB/Transregio 7. RG was supported by DFG GRK 1523, in particular during a stay at Princeton. FP was supported by NSF Grant No. PHY-0745779 and the Alfred P. Sloan Foundation. Computations were performed on JUROPA (Jülich) and at the LRZ (Munich).

[1] M. D. Duez, Class. Quant. Grav. **27**, 114002 (2010), 0912.3529.
[2] M. Shibata and K. Taniguchi, Living Reviews in Relativity **14** (2011).
[3] T. Baumgarte and S. Shapiro, Numerical Relativity (Cambridge University Press, Cambridge, 2010).
[4] K.-J. Jin and W.-M. Suen, Phys. Rev. Lett. **98**, 131101 (2007), gr-qc/0603094.
[5] T. Kellermann, L. Rezzolla, and D. Radice, Class. Quant. Grav. **27**, 235016 (2010), 1007.2797.
[6] M. Anderson, E. W. Hirschmann, L. Lehner, S. L. Liebling, P. M. Motl, D. Neilsen, C. Palenzuela, and J. E. Tohline, Phys. Rev. **D77**, 024006 (2008), 0708.2720.
[7] M. Miller, Phys. Rev. D **69**, 124013 (2004), gr-qc/0305024.
[8] M. Shibata, T. Nakamura, and K. Oohara, Prog. Theor. Phys. **89**, 809 (1993).
[9] I. Kowalska, T. Bulik, K. Belczynski, M. Dominik, and D. Gondek-Rosinska, Astron. Astrophys. **527**, A70 (2011), 1010.0511.
[10] R. M. O'Leary, B. Kocsis, and A. Loeb, MNRAS **395**, 2127 (2009), 0807.2638.
[11] W. H. Lee, E. Ramirez-Ruiz, and G. van de Ven, Astrophys. J. **720**, 953 (2010), 0909.2884.
[12] B. W. Murphy, H. N. Cohn, and P. M. Lugger, Astrophys. J. **732**, 67 (2011), 1205.1049.
[13] J. D. Dull, H. N. Cohn, P. M. Lugger, B. W. Murphy, P. O. Seitzer, P. J. Callanan, R. G. M. Rutten, and P. A. Charles, Astrophys. J. **585**, 598 (2003), arXiv:astro-ph/0210588.
[14] E. Pfahl, S. Rappaport, and P. Podsiadlowski, Astrophys. J. **573**, 283 (2002), arXiv:astro-ph/0106141.
[15] T. A. Thompson, Astrophys.J. **741**, 82 (2011), 1011.4322.
[16] J. P. Norris, N. Gehrels, and J. D. Scargle, Astrophys.J. **735**, 23 (2011), 1101.1648.
[17] B. C. Stephens, W. E. East, and F. Pretorius, Astrophys. J. **737**, L5 (2011), 1105.3175.
[18] P. C. Peters and J. Mathews, Phys. Rev. **131**, 435 (1963).
[19] M. Turner, Astrophys. J. **216**, 610 (1977).
[20] F. Pretorius and D. Khurana, Class. Quant. Grav. **24**, S83 (2007), gr-qc/0702084.
[21] U. Sperhake, E. Berti, V. Cardoso, J. A. González, B. Brügmann, and M. Ansorg, Phys. Rev. **D78**, 064069 (2008), 0710.3823.
[22] R. Gold and B. Brügmann, Class.Quant.Grav. **27**, 084035 (2010), 0911.3862.
[23] R. Gold and B. Brügmann (2012), 1209.4085.
[24] M. Turner, Astrophys. J. **216**, 914 (1977).
[25] K. D. Kokkotas and G. Schäfer, Mon. Not. Roy. Astron. Soc. **275**, 301 (1995), gr-qc/9502034.
[26] S. Rosswog, T. Piran, and E. Nakar (2012), 1204.6240.
[27] B. Brügmann, W. Tichy, and N. Jansen, Phys. Rev. Lett. **92**, 211101 (2004), gr-qc/0312112.
[28] B. Brügmann, J. A. González, M. Hannam, S. Husa, U. Sperhake, and W. Tichy, Phys. Rev. **D77**, 024027 (2008), gr-qc/0610128.
[29] M. Thierfelder, S. Bernuzzi, and B. Brügmann, Phys. Rev. D **84**, 044012 (2011), 1104.4751.
[30] W. E. East, F. M. Ramazanoglu, and F. Pretorius, Phys.Rev. **D86**, 104053 (2012), 1208.3473.
[31] N. Moldenhauer, Initial data for neutron star binaries (2012), Master Thesis, University of Jena.
[32] S. Bernuzzi, A. Nagar, M. Thierfelder, and B. Brügmann, Phys. Rev. D **86**, 044030 (2012), 1205.3403.
[33] J. Healy, J. Levin, and D. Shoemaker, Phys. Rev. Lett. **103**, 131101 (2009), 0907.0671.
[34] F. Pretorius (2007), 0710.1338.
[35] F. Löffler, L. Rezzolla, and M. Ansorg, Phys. Rev. D **74**, 104018 (2006), gr-qc/0606104.
[36] H. Dimmelmeier, N. Stergioulas, and J. A. Font, Mon.Not.Roy.Astron.Soc. **368**, 1609 (2006), astro-ph/0511394.
[37] L. Baiotti, S. Bernuzzi, G. Corvino, R. De Pietri, and A. Nagar, Phys. Rev. **D79**, 024002 (2009), 0808.4002.
[38] E. Gaertig and K. D. Kokkotas, Phys.Rev. **D83**, 064031 (2011), 1005.5228.
[39] W. C. G. Ho and D. Lai, Mon. Not. Roy. Astron. Soc. **308**, 153 (1999), astro-ph/9812116.
[40] W. E. East and F. Pretorius, Astrophys.J. **760**, L4 (2012), 1208.5279.